Semiclassical quantization of strongly chaotic vibrations in an M_7-like cluster

Atsuko Inoue-Ushiyama and Kazuo Takatsuka*
Department of Basic Science, Graduate School of Arts and Sciences, The University of Tokyo, Komaba, 153-8902, Tokyo, Japan
(Received 2 February 2001; published 24 October 2001)

We report semiclassical energy spectra of vibrational state of a cluster composed of seven identical atoms like Ar_7 in terms of our previously developed semiclassical wave function, which we call the action-decomposed function. The classical dynamics of this vibrational state is strongly chaotic and undergoes a large amplitude motion due to structural isomerization, which demands a long run of trajectory calculation. Permutation of identical particles should also be taken into account as a quantum effect, since a single molecular shape can be shared by many permutational isomers. Furthermore, chaos causes a spurious divergence in the amplitude factor of a correlation function in the initial value representation, which arises from the amplitude factor (prefactor) of a semiclassical wave function, while the final-state representation is suffered from the well-known divergence arising at caustics. Both approaches therefore face tremendous difficulty in a long-time calculation of the correlation functions. We challenge to extract some limited number of spectral lines from such chaotic dynamics. We further apply a correlation function that is free of such a troublesome amplitude factor. Numerical results from all these schemes are reported.

DOI: 10.1103/PhysRevE.64.056223 PACS number(s): 05.45.Mt, 03.65.Sq, 33.20.Tp, 36.40.−c

I. INTRODUCTION

Isomerization dynamics of clusters composed of identical atoms shows many quite interesting features that constitute some of the central notions in chemical dynamics. For instance, an M_7 cluster such as Ar_7 on the Lennard-Jones potential has four structural isomers having the corresponding potential basins (local minima), which are individually degenerate among the very many permutation isomers. This isomerization dynamics has been studied extensively from a view point of a microcanonical analog of the first-order solid-liquid phase transition [1]. The statistical properties arising from typically chaotic dynamics such as a Markov-type appearance of isomers in a high-energy region has been analyzed [2–6]. This isomerization dynamics may also be viewed as a prototype of high-energy multichannel chemical reactions in which multiple channels leading to different products are wide open [7]. A recent finding in this aspect is that the average lifetimes of the isomers bear an arrhenius-like relation with a temperature, called the local microcanonical temperature, that reflects a variational structure of the equi-energy plane in phase space for the individual potential basins [8].

It is extremely interesting and important to consider the quantum effects in the above cluster dynamics, since it can give a theoretical foundation of how the quantum effects can survive (or fade away) in mesoscopic systems. In particular, eigenfunctions arising from structural isomerization can reflect *superposition* of wave packets representing the individual molecular *shapes*. (We abbreviate it as *superposition of molecular shapes*.) Quantum mechanics thereby makes the classical notion of molecular shape vague. Besides, it is highly nontrivial how the quantum vibrational spectra of isomerization may be formed from the superposition of molecular shapes. With these analyses in mind as our final goal, we in this paper begin with an attempt of semiclassical evaluation of vibrational spectrum of an M_7-cluster up to an energy at which its classical counterpart undergoes structural isomerization.

A pioneering work about quantum effects on cluster dynamics was made by Leitner *et al.* [9] for Ar_3 in terms of the level statistics. Chakravarty *et al.* studied the effects of three-body forces on quantum chaos in rare-gas trimers [10]. Recently, quantum effects on large clusters have been explored within the framework of the quantum Monte Carlo method by Rick, Neirotti, and their coworkers [11,12]. The group of Chakravarty is also developing a path-integral Monte Carlo simulation method for clusters [13]. Our paper here is aimed at quantization of strongly chaotic vibrational states of a seven-particle cluster, covering a high-energy region, in which the Lindemann index suggests occurrence of structural isomerization.

It is expected that a full quantum calculation of the energy spectrum of such a large chaotic system is prohibitively difficult. Even the standard semiclassical theory [14–19] should be faced with extremely tough problems. A very rare exception is a recent work of Brewer *et al.* [20], who quantized a system of 15 coupled vibrational degrees of freedom. In the present paper, we apply a semiclassical wave function that has been developed and analyzed before by ourselves, which we call the action decomposed wave function (ADF) [21]. The ADF requires far less classical trajectories to calculate a time-correlation function, the Fourier transform of which gives rise to an energy spectrum. As a price, the ADF may sacrifice accuracy to some extent in case of a highly quantum system, for which action integrals are relatively small compared to the magnitude of the Planck constant.

As a report of this series of semiclassical studies on cluster dynamics, the present paper explores some basic subjects that should be taken into account in actual numerical calculations. The classical dynamics of an M_7 cluster is hence revisited from another point of view. For instance, the pat-

*Corresponding author. Email address: kaztak@mns2.c.u-tokyo.ac.jp

tern of isomerizations is to be classified in the context of particle permutation. Also, the local K entropy proposed by Hinde, Berry, and Wales [22,23] is viewed as a quantity that practically limits the time length of the time-correlation function.

The semiclassical theory based on the ADF is also re-examined so as to cope with strong chaos in a large system. The main difficulty is spurious divergence in the amplitude factor (prefactor) of semiclassical wave functions or the kernel: not only the well-known divergence at caustics [16,19] in the final value representation (FVR), but also an exponential growth of the amplitude factor in the initial value representation (IVR). (See Refs. [24–30] for the initial and final value representations of the semiclassical kernels.) Both of the divergences impose tough restrictions on the practical integration of the correlation function. We here manage to extract the spectral information as much as possible.

Nevertheless, the spectrum we can obtain by a tactical application of both the IVR and FVR is limited in an energy range where the exponential growth of the amplitude factor in the IVR is sufficiently slow. We therefore apply our previously formulated correlation function that is free of the amplitude factor [31]. Numerical results with this correlation function are also reported.

The present paper is organized as follows. In Sec. II, classical dynamics of an M_7 cluster is re-examined from a viewpoint of semiclassical application. The first half of Sec. III briefly reviews the Maslov-type semiclassical theory and then it is extended to take account of permutation of identical particles. The last half presents some numerical results of vibrational spectrum. In Sec. IV, we show the numerical results given by the amplitude-free correlation function. This paper concludes in Sec. V with some remarks.

II. CLASSICAL DYNAMICS OF CLUSTER ISOMERIZATION

We first review the classical dynamics of clusters bound by the Morse potential, which undergo isomerization and highly chaotic motion. A special focus is placed on practical problems for semiclassical quantization. Many other interesting features may be found by consulting papers by the groups of Berry and Wales [1] and our previous papers [2–8].

A. System

A classical Hamiltonian of a cluster composed of seven identical atoms has the following canonical form:

$$H=\frac{m}{2}\sum_{i=1}^{7}\left[\left(\frac{dx_i}{dt}\right)^2+\left(\frac{dy_i}{dt}\right)^2+\left(\frac{dz_i}{dt}\right)^2\right]+\varepsilon\sum_{i<j}\left(e^{-2\beta(r_{ij}-r_0)}-2e^{-\beta(r_{ij}-r_0)}\right), \tag{1}$$

where r_{ij} represents the distance between atoms i and j. The potential parameters r_0, ε, and β are the equilibrium distance, potential depth, and the ''range'' of the isolated diatomic molecule. With the following rescaling:

$$\beta x\to\tilde{x},\quad \beta y\to\tilde{y},\quad \beta z\to\tilde{z},$$

$$\beta r_{ij}\to\rho_{ij},\quad \beta r_0\to\rho_0,\quad \left(\frac{\varepsilon\beta^2}{m}\right)^{1/2}t\to\tau, \tag{2}$$

the total Hamiltonian is transformed to the dimensionless form

$$\frac{H}{\varepsilon}=\frac{1}{2}\sum_{i=1}^{7}\left[\left(\frac{d\tilde{x}_i}{d\tau}\right)^2+\left(\frac{d\tilde{y}_i}{d\tau}\right)^2+\left(\frac{d\tilde{z}_i}{d\tau}\right)^2\right]+\sum_{i<j}\left(e^{-2(\rho_{ij}-\rho_0)}-2e^{-(\rho_{ij}-\rho_0)}\right). \tag{3}$$

In what follows, our numerical results are all represented in these dimensionless (absolute) units. In Eq. (3), only one parameter ρ_0 is left to control the Hamiltonian. The range of physically accessible ρ_0 is [32] about $1.5<\rho_0<7.0$.

Braier and Berry [32] have studied the effects of the potential range ρ_0 in the above Morse function, deducing the following qualitative results: The number of distinct potential minima and transition states depends on ρ_0; the larger is ρ_0, the shorter (more compact) is the potential range and the more are geometrically different potential minima. For example, the Ar_7 cluster, to which $\rho_0=6.0$ should be assigned, has four stable local structures (isomers) as in the Lennard-Jones potential [33]. These stable structures are labeled pentagonal bipyramid (PBP), capped octahedron (COCT), tricapped tetrahedron, and bicapped trigonal bipyramid (SKEW) with the potential minimum of -16.208ε, -15.564ε, -15.248ε, and -15.216ε, respectively. On the other hand, for smaller ρ_0, say, $\rho_0=3.0$, only two structures, the PBP and COCT are present. The energies at the bottom of their basins are -17.553ε and -17.276ε, respectively. (See Ref. [5] for the dependence of dynamics on ρ_0.) To identify the molecular structure among possible isomers, it is a usual practice to use the so-called quenching technique due to Stillinger and Weber [34].

In what follows, we confine ourselves to a system of $\rho_0=3.0$ to quantize the vibrational states under a rather simple situation as stated above. In this M_7-like system of appropriate molecular parameters (r_0, ε, and β), the unit time approximately corresponds to 0.8 ps, and the Plank constant is about 0.08. The relative energy is to be measured from the bottom of the PBP structure -17.553ε.

B. Isomerization

It is well known from cumulative studies on small clusters [1,33,35,36] that a single cluster, such as the Ar_7-like cluster, undergoes ''melting'' from solidlike to liquidlike states as the total energy increases. Such a transition may be well monitored by the Lindemann index

$$\delta=\frac{2}{N(N-1)}\sum_{i<j}\frac{(\langle r_{ij}^2\rangle_t-\langle r_{ij}\rangle_t^2)^{1/2}}{\langle r_{ij}\rangle_t}, \tag{4}$$

which detects the stiffness of a cluster by measuring the deviation of the bond length from their average values. Here, in Eq. (4), N is the number of composite particles, r_{ij} is a dis-

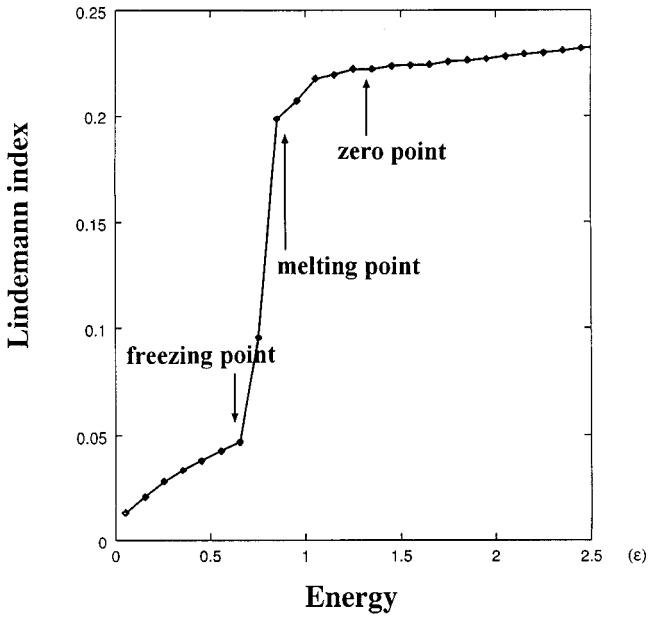

FIG. 1. The Lindemann index versus the total energy of the M_7 cluster ($\rho_0=3.0$) in absolute units. The freezing and melting points are about 0.6ε and 1.1ε, respectively.

tance between the ith and jth particles, and $\langle\,\rangle_t$ means a time average. The time interval over which to take the average is usually taken to be long enough to attain a converge.

Figure 1 shows the Lindemann curve starting from the PBP basin. Three stages are observed; the ''solidlike'' phase below about 0.6ε that is called ''freezing point,'' and the ''liquidlike'' phase above about 1.1ε called ''melting point,'' and the coexistence region in between. Below the freezing point, a cluster displays a bounded motion (small and local oscillation) in the PBP basin and seldom comes out of the basin. As the total energy increases over the melting point, a drastic structural change, namely, the transition from one basin to another begins to start. Therefore, the bound states above the freezing point must be generated by trajectories undergoing isomerization.

The periods of the vibrational motions in the solidlike state (low-energy extreme) are often estimated in terms of the normal modes at the bottoms of the basins. In Table I, the frequencies, periods, and eigenenergies thus obtained for the PBP basin are listed. The period of the PBP structure ranges from 2.050τ to 5.955τ (from 1.654 to 4.806 ps) and the eigenenergy from 0.086ε to 0.249ε. The zero-point energy of this system in the *harmonic approximation* is then given as high as 1.2849ε, which is higher than the melting energy (1.1ε). This fact simply indicates that the present molecule is far from a harmonic system. Similarly, Leitner *et al.* [9] found that the zero-point energy of the Ar_3 cluster was already in the energy range of classical chaos.

The dissociation energy of the present M_7 cluster is roughly estimated as 9.0ε, which is much higher than the melting energy and therefore even higher than that of the transition state. Although the cluster dissociates directly with an energy higher than 12.0ε, those in between 9.0ε and 12.0ε remain bounded with a long induction time before dissociation.

TABLE I. Frequencies, periods, and assumed eigenenergies of the normal modes.

Frequency (τ^{-1})	Period (τ)	Period (ps)	Eigenenergy (ε)
3.063	2.050	1.654	0.249
3.038	2.069	1.669	0.247
3.038	2.069	1.669	0.247
2.743	2.291	1.849	0.223
2.743	2.291	1.849	0.223
2.386	2.631	2.123	0.194
2.386	2.631	2.123	0.194
2.226	2.816	2.273	0.181
1.697	3.706	2.991	0.138
1.697	3.706	2.991	0.138
1.500	4.196	3.386	0.122
1.500	4.196	3.386	0.122
1.464	4.280	3.454	0.119
1.058	5.955	4.806	0.086
1.058	5.955	4.806	0.086

C. Two types of isomerization and permutation of atoms

One of the important quantum effects in the study of clusters composed of identical atoms is the permutation symmetry. There are quite a lot of permutation isomers, which roughly amounts to the order of 7! for a M_7 cluster for individual structural isomers. (Note that the number of the permutation isomers heavily depends on the molecular symmetry, although semiclassical quantization does not care about instantaneous molecular symmetries appearing along classical trajectories.) Since the quenching method [34] alone does not distinguish permutation isomers, we need a conventional indicator to identify them. A method devised by Sawada and Sugano using a distance index should work well for this purpose [37]. We here consider a similar method.

Let $\mathbf{q}_t$ be a point of a classical trajectory at time t in $3N$-dimensional Cartesian configuration space. (However, we actually fix the motion of the center of mass and the total rotation.) A point $\mathbf{q}_t$ also specifies the molecular geometry by identifying the potential basin [34]. Then, the molecular size at each time may be measured with a hyper-radius $R(\mathbf{q}_t)$

$$R(\mathbf{q}_t)=|\mathbf{q}_t-\mathbf{q}_{\mathrm{PBP}}|, \tag{5}$$

where, for instance, $\mathbf{q}_{\mathrm{PBP}}$ denotes the molecular configuration at the bottom of the PBP basin. For a given coordinate $\mathbf{q}_t$, one may create its permutation isomers $\hat{P}_i\mathbf{q}_t$ $(i=1,\ldots,7!)$ by applying the permutation operators $\hat{P}_i$ on the atomic coordinates. It is obvious that operation of $\hat{P}_i$ does not change the potential and geometry. However, $|\hat{P}_i\mathbf{q}_t-\mathbf{q}_{\mathrm{PBP}}|$ may be different from each other. Then let us assume a trajectory that starts from the PBP basin and comes back to the PBP basin with an atomic permutation after a series of isomerizations. It is then expected that

$$|\mathbf{q}_t-\mathbf{q}_{\mathrm{PBP}}|\gg|\mathbf{q}_{t=0}-\mathbf{q}_{\mathrm{PBP}}|. \tag{6}$$

On the other hand, one may find a permutation operator $\hat{P}_j$ that recovers

$$|\hat{P}_j \mathbf{q}_t - \mathbf{q}_{\mathrm{PBP}}| = |\mathbf{q}_t - \hat{P}_j^{-1} \mathbf{q}_{\mathrm{PBP}}| \simeq |\mathbf{q}_{t=0} - \mathbf{q}_{\mathrm{PBP}}|. \tag{7}$$

Thus, if such a $\hat{P}_j$ is found, we can approximately judge that a cluster has undergone a permutation after isomerization. Since it is tedious to find such a $\hat{P}_j$, we alternatively determine the following distance along a trajectory, which we call the shape distance, as

$$R_p(\mathbf{q}_t) = \min\{|\hat{P}_i \mathbf{q}_t - \mathbf{q}_{\mathrm{PBP}}| \,|\, i = 1, \ldots, 7!\}. \tag{8}$$

Thus, if

$$R(\mathbf{q}_t) = |\mathbf{q}_t - \mathbf{q}_{\mathrm{PBP}}| \gg R_p(\mathbf{q}_t) \tag{9}$$

is observed, we judge that a permutation has occurred.

Detecting the occurrence of permutation isomerization is one thing and incorporating the effect of permutation explicitly in the semiclassical theory is another, since we will do so without the use of $R(\mathbf{q}_t)$ or $R_p(\mathbf{q}_t)$ as shown in the next section. However, one may say that if such permutations occur frequently, the quantum effect due to permutation symmetry (boson or fermion) should be taken into account. If, conversely, permutation isomerization rarely occurs in classical dynamics, this quantum effect on a spectrum should not be significant. We will show that this is really the case in the next section.

We next show selected examples to see how often permutations may occur after structural isomerizations. $R_p(\mathbf{q}_t)$ and $R(\mathbf{q}_t)$ for trajectories of three different energy 0.18ε, 1.12ε, and 3.82ε are sampled in Fig. 2. It is observed that (a) R_p does not become larger than about 5, and (b) $R_p(\mathbf{q}_t) = R(\mathbf{q}_t)$ for trajectories in lower energy ($\sim 2.5\varepsilon$ for $t < 100\tau$). It is thus observed that $R_p(\mathbf{q}_t)$ and $R(\mathbf{q}_t)$ are mutually similar for lower-energy trajectories (0.18ε and 1.12ε), while they deviate significantly from each other for the high-energy trajectory (3.82ε). It turns out numerically that in the energy lower than $\sim 2.5\varepsilon$, a cluster getting out of a basin returns mostly to the permutationally same basin as it was before isomerization (note that the melting energy is about 1.1ε). This motion is called swinging motion. On the other hand, if the total energy exceeds $\sim 2.5\varepsilon$, a cluster becomes to start a long journey, wanders among basins, and comes back to the same shape but in a permutationally different basin. We call such a motion ''wandering motion.'' Trajectories of wandering motion should be required to take account of permutation of particles for a quantum correlation function to be able to count a correct value. In other words, the quantum effect arising from the particle permutation should become vital in quantizing such high-energy states. On the other hand, for a quantum system whose main contributions come from the swinging motion, the permutation symmetry must play only a marginal role.

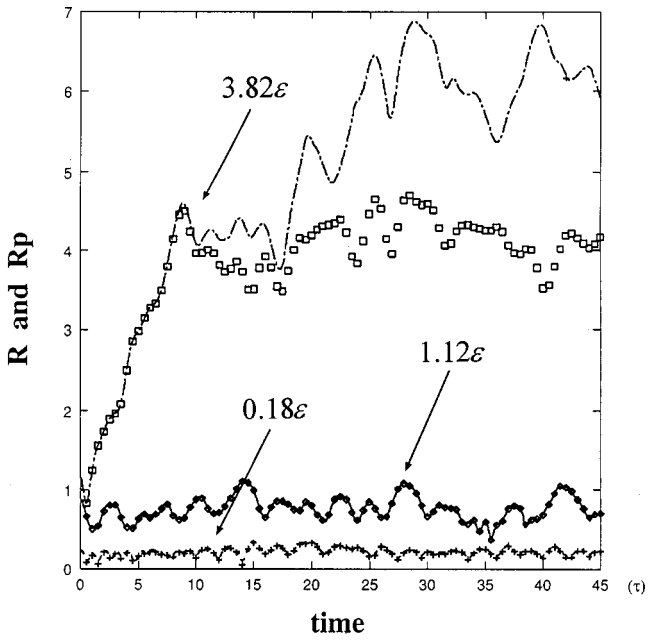

FIG. 2. The hyper-radius (curves) and shape distance (points indicated with squares and so on) for selected trajectories in absolute units. For trajectories of energies as low as 0.18ε and 1.12ε, the shape distance continues to coincide with the hyper-radius, whereas the high-energy trajectory is associated with a large deviation between the two. The latter indicates an occurrence of permutation isomerization.

D. Measure of the extent of chaos

In our semiclassical approximation arises an amplitude factor $|\partial \mathbf{q}_t / \partial \mathbf{q}_0|^{1/2}$ along a trajectory [see Eq. (41)]. This value generally oscillates but its envelope grows exponentially in a strongly chaotic system, which deteriorates the semiclassical approximation. We, thus, should check the rate of this divergence beforehand. A standard way to measure the instability of a classical trajectory is to calculate the eigenvalues of the so-called stability matrix [38–40] $\mathbf{Z}$,

$$\mathbf{Z} = \left[\frac{\partial(\mathbf{q}_t, \mathbf{p}_t)}{\partial(\mathbf{q}_0, \mathbf{p}_0)} \right], \tag{10}$$

which satisfies the following equation of motion,

$$\dot{\mathbf{Z}} = \mathbf{JHZ}, \tag{11}$$

where $\mathbf{H}$ is the Hessian matrix of the classical Hamiltonian and the symplectic matrix $\mathbf{J}$ is

$$\mathbf{J} = \begin{pmatrix} \mathbf{0} & \mathbf{1} \\ -\mathbf{1} & \mathbf{0} \end{pmatrix}. \tag{12}$$

(See Ref. [41] for an accurate calculation of $\mathbf{Z}$.) From Eq. (11), the equation of motion for one of the submatrices,

$$\mathbf{D} \equiv [\partial \mathbf{q}_t / \partial \mathbf{q}_0], \tag{13}$$

is obtained in the following form:

$$\ddot{\mathbf{D}} = -\mathbf{V}\mathbf{D}, \tag{14}$$

where $\mathbf{V}$ is the Hessian of the potential, namely,

$$\mathbf{V} = \frac{\partial V}{\partial \mathbf{q}_t \partial \mathbf{q}_t}. \tag{15}$$

With the diagonal matrix $\Lambda \equiv \mathbf{U}(-\mathbf{H}_{xx})\mathbf{U}^{-1}$, Eq. (14) is represented as

$$\mathbf{U}\ddot{\mathbf{D}}\mathbf{U}^{-1} = \Lambda(\mathbf{U}\mathbf{D}\mathbf{U}^{-1}). \tag{16}$$

Consequently, the determinant of matrix $(\mathbf{U}\mathbf{D}\mathbf{U}^{-1})$, namely, $D = \det(\mathbf{D})$ is *roughly* estimated as

$$D \sim e^{\int [\alpha(t) + i\beta(t)]dt}, \tag{17}$$

where α and β denote the sum over the square root of the positive and negative eigenvalues, respectively, of Λ at each time. That is, the average value of α is regarded as the Kolmogolov entropy at time t, so that

$$D \sim \exp[\bar{K}t], \tag{18}$$

where $\bar{K}$ is a time average of $\alpha(t)$.

The local K entropy due to Hinde *et al.* and Hinde and Berry [22,23] is a quantity that represents the magnitude of the negative curvature at a point on the potential-energy surface, defined as

$$K = \sum_{\omega_j^2 < 0} |\omega_j^2|^{1/2}, \tag{19}$$

where ω_j^2 denotes the eigenvalue of the local Hessian matrix of the potential function V. (Here, we have disregarded a factor $1/\log_{10} 2$ appearing in the original definition [22,23]). A trajectory becomes unstable when it passes over a negatively curved portion of the potential-energy surface. The larger K indicates the more separation in the bundle of trajectories. $\bar{K}$ defined above is essentially the same quantity as K. More precisely, the time average of the local K entropy along the trajectory

$$\langle K \rangle_t = \frac{1}{T}\int_0^T K dt = \frac{1}{T}\sum_{i=1}^{T/\triangle t} K \triangle t \tag{20}$$

is regarded as $\bar{K}$ for simplicity.

Figure 3 shows the time averaged local K entropy from 10 000 sample trajectories, where the time averaging is carried out with $\triangle t = 0.5\tau$ and $T = 1000\tau$. It is seen that $\langle K \rangle_t$ becomes larger almost linearly with the total energy in the range from about 1ε up to 8ε. The abrupt fall seen in the very high-energy region beyond $8\varepsilon \sim 9\varepsilon$ is due to dissociation (break) of the clusters. In addition, it has been numerically confirmed that $\langle K \rangle_t$ does not strongly depend on T and $\triangle t$ in the energy range $[\sim 1\varepsilon, \ \sim 8\varepsilon]$. Thus, we see that the present system exhibits a strong and ''uniform chaos.'' By uniform we mean that the local K entropy depends on the total energy alone but not much on the individual trajectories

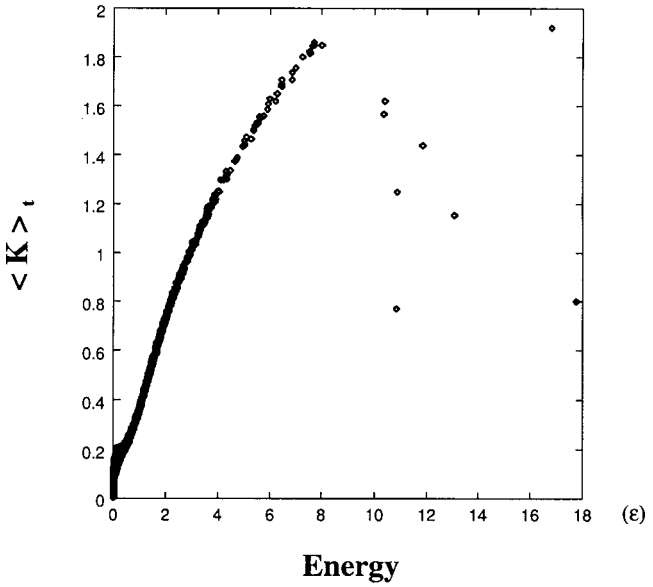

FIG. 3. The local K entropy vs the total energy in units of ε, averaged over 10 000 trajectories.

and the length of the integration time. Below the melting point (about 1.1ε), however, the behavior of $\langle K \rangle_t$ is rather complicated (see Fig. 3). In fact, the energy dependence of the K entropy in Ar_3 is reported to be not monotonic around the energy range of phase change [9]. Berry and his coworkers and Hinde and Berry have analyzed the local K entropy by comparing it with the potential topography, and found a remarkable fact that it takes relatively small value (suggesting dynamical stability) around the transition states [1,22,23].

As seen in Fig. 3, $\bar{K}$ ranges from 0 to 2 for the M_7-like cluster with the total energy up to the dissociation limit 9.0ε. Thus, the magnitude of D in Eq. (18) may range from the order of 10^0 to 10^{200} in $t = 100\tau$, depending on the total energy. In evaluating the semiclassical correlation function, many trajectories having different energies and such tremendously different magnitudes in the amplitude have to be taken into account [see Eq. (28)], which causes a serious difficulty in the numerical integration.

III. SEMICLASSICAL VIBRATIONAL SPECTRA WITH THE ACTION DECOMPOSED FUNCTION

We next present a brief review of the formulation of a Maslov-type semiclassical wave function, with which we calculate the correlation functions [21]. An extension to take account of the permutation is made.

A. The action decomposed function

Maslov and Feodoriuk [17] have established a systematic theory to generate a class of wave functions in the form of

$$\Psi(q,t) = F(q,t)\exp\left[\frac{i}{\hbar}S_{cl}\right], \tag{21}$$

where S_{cl} denotes the classical action satisfying the Hamilton-Jacobi equation

$$\frac{\partial S_{cl}}{\partial t}+H\left(q,\frac{\partial S_{cl}}{\partial q},t\right)=0. \tag{22}$$

The lowest-order semiclassical equation of motion for the amplitude function $F(q,t)$ is

$$\frac{\partial F}{\partial t}+v\cdot\nabla F+\frac{1}{2}(\nabla\cdot v)F=0, \tag{23}$$

which has neglected $(i\hbar/2)\nabla^2 F$ from the right-hand side of the full (rigorous) equation of motion for F. An explicit solution to Eq. (23) may be readily obtained as

$$F(q_t,t)=F(q_0,0)\left(\frac{\partial q_t}{\partial q_0}\right)^{-1/2}=F(q_0,0)\left|\frac{\partial q_t}{\partial q_0}\right|^{-1/2}\times\exp\left[-\frac{i\pi M}{2}\right], \tag{24}$$

where the Jacobian determinant $\partial q_t/\partial q_0$ is taken under a fixed initial momentum p_0, and M is the Maslov index in this representation that counts the number of zeros of $\partial q_t/\partial q_0$ up to degeneracy [16]. The classical action in Eq. (21) has naturally been chosen as the F_2-type generating function of Goldstein [42] (denoted as S_2 hereafter). In other words, all the classical paths representing Eq. (21) lie on a single action surface, the initial momentum of which is p_0 everywhere. This is why we call this function as the action-decomposed function (ADF). Having this action function as a phase, the initial form of ADF at $t=0$ is rewritten as

$$\Psi_{p_0}(q,t)=F(q,0)\exp\left[\frac{i}{\hbar}p_0 q\right]. \tag{25}$$

Any arbitrary wave function may be expanded in terms of the ADF's (see below). Among others, a wave function that consists of a single ADF is called single ADF (SADF). A SADF is rewritten in a little more global form as

$$\Psi_{p_0}(q,t)=\int dq_t\,\delta(q-q_t)F(q_0,t)\times\left|\frac{\partial q_t}{\partial q_0}\right|^{-1/2}\exp\left[\frac{i}{\hbar}S_2(q_t,p_0;t)-\frac{i\pi M}{2}\right]. \tag{26}$$

For the later convenience, we also call this the final value representation (FVR). As is well known, the amplitude factor $|\partial q_t/\partial q_0|^{-1/2}$ diverges at every caustic, where $\partial q_t/\partial q_0=0$. Besides, the sampling of trajectories is not easy to have the integral of Eq. (26) be accurate, since the points q_t result only after running trajectories of $p(0)=p_0$. They are not necessarily good quadrature points. To overcome these difficulties, one may transform the integration variables as

$$\int\cdots dq_t=\int\cdots\left|\frac{\partial q_t}{\partial q_0}\right|dq_0, \tag{27}$$

which was first proposed by Miller [24] to treat the Feynman kernel in the initial value representation (IVR). The result is

$$\Psi_{p_0}(q,t)=\int dq_0\,\delta[q-q_t(q_0,p_0)]F(q_0,t)\times\left|\frac{\partial q_t}{\partial q_0}\right|^{1/2}\exp\left[\frac{i}{\hbar}S_2(q_t,p_0;t)-\frac{i\pi M}{2}\right]. \tag{28}$$

After Miller we call this form the IVR. In this representation, the initial sampling is much easier, and the amplitude factor $|\partial q_t/\partial q_0|^{1/2}$ becomes zero at caustics.

B. Propagation of an arbitrary wave function in terms of ADF

An arbitrary wave function may be evolved in time in terms of the ADF as follows [21]. Suppose we have a decomposition for an arbitrary wave function such that

$$\Psi(q)=F(q)G(q), \tag{29}$$

under a condition that $G(q)$ has a momentum representation

$$\tilde{G}(p)=\frac{1}{(2\pi\hbar)^N}\int G(q)\exp\left(-\frac{i}{\hbar}pq\right)dq. \tag{30}$$

We assume that $F(q)$ is a slowly varying function in q space. The total wave function thus decomposed is rewritten as

$$\Psi(q)=\int dp_0\tilde{G}(p_0)F(q)\exp\left(\frac{i}{\hbar}p_0 q\right), \tag{31}$$

which is regarded as a superposition of many ADF's of Eq. (25). The semiclassical time propagation of this wave function is described in a straightforward manner as

$$\Psi(q)=\int dp_0\tilde{G}(p_0)\int dq_t\,\delta(q-q_t)F(q_0,0)\left|\frac{\partial q_t}{\partial q_0}\right|^{-1/2}\times\exp\left[-\frac{i\pi M}{2}\right], \tag{32}$$

where $q_0=\partial S_2(q,p_0;t=0)/\partial p_0$.

As an extreme example of this wave function, the semiclassical Feynman kernel in the coordinate-momentum representation $\langle q|\exp[-(i/\hbar)Ht]|p_0\rangle=K(q,p_0;t)$ is reproduced by setting

$$F(q)=1\ \ (\text{constant});\quad G(q)=\Psi(q)(\text{wave function itself}), \tag{33}$$

and hence,

$$\tilde{G}(p)=\tilde{\Psi}(p)\times(\text{momentum representation of the wave function}). \tag{34}$$

We then have

$$\Psi(q,t)=\frac{1}{(2\pi\hbar)^N}\int\int dq_0dp_0\delta(q-q_t)\left|\frac{\partial q_t}{\partial q_0}\right|^{1/2}\times\exp\left[-\frac{i\pi M}{2}\right]\exp\left[\frac{i}{\hbar}S_2(q_t,p_0;t)\right]\tilde{\Psi}(p_0). \tag{35}$$

This is nothing but

$$\Psi(q,t)=\int dp_0K(q,p_0;t)\tilde{\Psi}(p_0) \tag{36}$$

except for a minor difference in the constant phase factor.

The other extreme side of the action decomposition is the single action-decomposed function (SADF). Let

$$F=F(q)G=\exp\left(\frac{i}{\hbar}p_0q\right),\quad \tilde{G}(p)=\delta(p-p_0), \tag{37}$$

and we simply come back to Eq. (28). The most significant difference between the kernel and SADF is in the distribution in momentum space, namely, Eqs. (34) and (37).

C. Correlation function with SADF

As was stressed previously [21], difference in the dimensionality of the integrals of Eqs. (28) and (35) is enormous. The former expression involves only N-dimensional integral, while the latter does $2N$-dimensional integral. A price is that the SADF is a little less accurate, but it performs much faster convergence with respect to the number of classical trajectories required. In fact, the efficiency of the SADF has been numerically evidenced under certain conditions [21]. That is, if the Planck constant is small, and/or when a potential under study is anharmonic, the SADF may reproduce sufficiently accurate quantum energy spectra with far fewer classical trajectories than those that are required by the semiclassical kernel. Since the M_7 system is very large from the viewpoint of quantum and semiclassical dynamics, we confine our following calculations only to the SADF scheme.

A time-correlation function represented in the SADF is

$$C(t)=\langle\Psi_{p_0}(0)|\Psi_{p_0}(t)\rangle=\int dq_0F^*(q_t,0)F(q_0,0)\times\left|\frac{\partial q_t}{\partial q_0}\right|^{1/2}\exp\left[-\frac{i}{\hbar}p_0q_t+\frac{i}{\hbar}S_2(q_t,p_0;t)-\frac{i\pi M}{2}\right]. \tag{38}$$

Again, this expression involves only an N-dimensional integration. This is in a marked contrast to the correlation function represented in terms of the semiclassical Feynman kernel, which consists of at least $2N$-fold integrals. Therefore, the SADF is anticipated to provide quantum spectra with far fewer classical trajectories. On the other hand, the SADF has a clear limitation beyond which the theory is not valid. Taking this limitation into care, however, one may utilize the SADF as a very powerful tool to calculate spectra of rather large systems.

The energy spectrum may be extracted from the Fourier transform of the time-correlation function $C(t)=\langle\Psi(0)|\Psi(t)\rangle$,

$$S(E)=\frac{1}{2\pi\hbar}\int C(t)\exp\left[\frac{iEt}{\hbar}\right]dt. \tag{39}$$

$C(t)$ is written with a SADF such that

$$C_{FVR}(t)=\langle\Psi_{p_0}(0)|\Psi_{p_0}(t)\rangle=\int dq_tF^*(q_t,0)F(q_0,0)\times\left|\frac{\partial q_t}{\partial q_0}\right|^{-1/2}\exp\left[\frac{i}{\hbar}S_2(q_t,p_0;t)-\frac{i}{\hbar}p_0q_t-\frac{i\pi M}{2}\right] \tag{40}$$

in the FVR or

$$C_{IVR}(t)=\int dq_0F^*(q_t,0)F(q_0,0)\left|\frac{\partial q_t}{\partial q_0}\right|^{1/2}\exp\left[\frac{i}{\hbar}S_2(q_t,p_0;t)-\frac{i}{\hbar}p_0q_t-\frac{i\pi M}{2}\right] \tag{41}$$

in the IVR.

D. Permutation symmetry in semiclassical correlation function

We next treat the permutation of identical particles in a simplified way. A wave function, symmetrized or antisymmetrized, should have the form

$$\Psi=\frac{1}{\sqrt{N!}}\sum_{i=1}^{N!}\epsilon_i\hat{P}_i\Phi(\mathbf{x}_1,\ldots,\mathbf{x}_N)\equiv\mathbf{P}\Phi(\mathbf{x}_1,\ldots,\mathbf{x}_N), \tag{42}$$

where $\Phi(\mathbf{x}_1,\ldots,\mathbf{x}_N)$ is a primitive function to be symmetrized. $\hat{P}_i$ $(i=1,\ldots,N!)$ denote all the possible permutations, and ϵ_{p_i} are their associated parity. $\epsilon_{p_i}=-1$ for odd permutations for fermions, and otherwise they are simply positive unity. For bosons, $\epsilon_{p_i}=1$. The time-correlation function for such a symmetrized wave function is written as

$$\langle\Psi(0)|\Psi(t)\rangle=\left\langle\mathbf{P}\Phi(0)\left|\exp\left[-\frac{i}{\hbar}Ht\right]\right|\mathbf{P}\Phi(0)\right\rangle. \tag{43}$$

Since $\mathbf{P}$ commutes with the Hamiltonian H, and with the help of a relation $\mathbf{P}^2=\sqrt{N!}\mathbf{P}$, Eq. (43) may be written as

$$\langle\Psi(0)|\Psi(t)\rangle=\left\langle\mathbf{P}^2\Phi(0)\left|\exp\left[-\frac{i}{\hbar}Ht\right]\right|\Phi(0)\right\rangle=\sqrt{N!}\langle\mathbf{P}\Phi(0)|\Phi(t)\rangle. \tag{44}$$

This way of incorporating the permutation is particularly convenient, since one does not have to care about permutation in propagating a primitive wave function $\Phi(t)$. The symmetry operation comes in only when we take an overlap integral after the time propagation. As an example, let $\Phi_0(\mathbf{q})$ be an initial Gaussian function

$$\Phi_0(\mathbf{q}) = \mathcal{N}\exp\left[-\frac{\alpha}{2}(\mathbf{q}-\mathbf{q}_c)^2\right] \equiv \mathcal{N}\exp\left[-\frac{\alpha}{2}R^2(\mathbf{q})\right]. \tag{45}$$

Then, our semiclassical time-correlation function is written as

$$\begin{aligned}\langle\Psi(0)|\Psi(t)\rangle &= \int dq_t \sqrt{N!}\times\{\mathbf{P}\Phi_0^*(q_t)\}\Phi(q_t,t)\\ &= \mathcal{N}^2\int dq_t \sum_{i=1}^{N!}\left(\epsilon_{p_i}\hat{P}_i\exp\left[-\frac{\alpha}{2}R^2(q_t)\right]\right)\\ &\quad\times\left|\frac{\partial q_t}{\partial q_0}\right|^{-1/2}\exp\left[-\frac{\alpha}{2}R^2(q_0)\right]\exp\left[\frac{i}{\hbar}S_2(q_t)\right.\\ &\quad\left.-\frac{i\pi M}{2}\right].\end{aligned} \tag{46}$$

Thus, it is sufficient to operate the permutation operators only to $\Phi_0^*(\mathbf{q}_t)$, which is not propagated semiclassically. The corresponding correlation function disregarding the permutation is

$$\begin{aligned}\langle\Psi(0)|\Psi(t)\rangle &= \mathcal{N}^2\int dq_t \exp\left[-\frac{\alpha}{2}R^2(q_t)\right]\left|\frac{\partial q_t}{\partial q_0}\right|^{-1/2}\\ &\quad\times\exp\left[-\frac{\alpha}{2}R^2(q_0)\right]\exp\left[-\frac{i}{\hbar}S_2(q_t)\right.\\ &\quad\left.-\frac{i\pi M}{2}\right].\end{aligned} \tag{47}$$

Through comparison between Eqs. (46) and (47), it is therefore readily predicted that the time-correlation function is considerably underestimated without the permutation when the shape distance is shorter than the simple hyper-radius is, as in Eq. (9).

E. On tunneling trajectories

One may incorporate the tunneling effects to all the semiclassical theories described above and the amplitude-free correlation function to be discussed below. We have previously proposed a semiclassical tunneling theory by finding nonclassical paths in the real-valued configuration space along which complex-valued solutions to the Hamilton-Jacobi equation is generated [43]. These paths may be adopted into any semiclassical theory [44]. Without these nonclassical paths, neither potential tunneling nor dynamical tunneling [45] is taken into account well, and therefore, the tunneling splitting is not produced. In the present paper, however, we do not intend to consider such nonclassical paths in the calculations of the semiclassical correlation functions, simply because our system is highly chaotic and since we are mainly interested in relatively high-energy dynamics. We here avoid adding complexity to such an already complicated dynamic. This aspect is a subject in our future work.

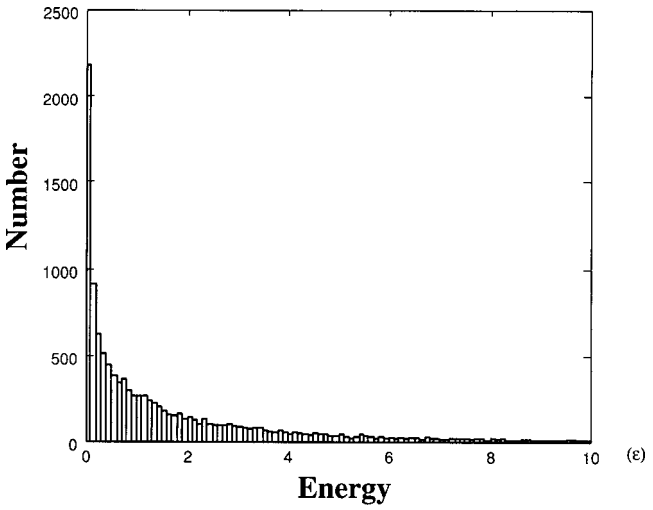

FIG. 4. Energy distribution arising from the multidimensional importance sampling to represent the initial Gaussian wave packet in absolute units.

F. Spectra

We now show numerical results for semiclassical quantization of the M_7 cluster, to which the single action-decomposed function (SADF) is applied. An action surface $\mathbf{p}_0=0$ is selected to generate an SADF. The Gaussian wave packet is adopted as an initial wave packet with the form

$$\Phi_0(\mathbf{q}) = \mathcal{N}\exp\left[-\frac{\alpha}{2}(\mathbf{q}-\mathbf{q}_c)^2\right], \tag{48}$$

where the center of the Gaussian $\mathbf{q}_c$ is located at the bottom of the PBP basin. The parameter α is chosen to be unity that is small enough for the SADF to be valid. This value $\alpha=1$, is actually far smaller than the exponent of an assumed eigenfunction of the lowest normal mode in Table I, which corresponds to $\alpha\sim 13$.

The numerical integration in Eq. (41) has been carried out with the multidimensional Monte Carlo integration, in which the initial configurations $\mathbf{q}_0$ are picked by means of a multidimensional importance sampling method. The importance sampling is indispensable to avoid energies high enough for the cluster to dissociate. The translational and the rotational momentum of the cluster is set to 0. Figure 4 shows the energy distribution of 16 000 classical trajectories thus obtained. The number of samples decrease as the energy becomes higher according to the weighting function. Nonetheless, the energy distribution has a long tail that reaches the dissociation limit. The wide range of energy may be necessary to obtain accurate spectra on one hand, but the high energy components necessarily bring about an extremely difficult practice on the other.

1. Initial value representation and divergence due to chaos

We first attempt to take a Fourier spectrum from the correlation function in the initial value representation, Eq. (41). As noted above, the amplitude factor $D^{1/2}=|\partial\mathbf{q}_t/\partial\mathbf{q}_0|^{1/2}$ behaves as $D\sim\exp[\bar{K}t]$, although it is free from divergence at

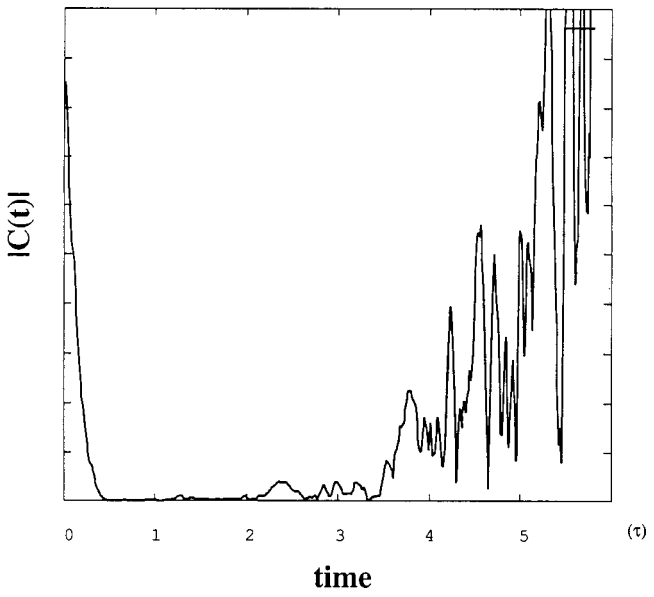

FIG. 5. The time evolution of the absolute value of an autocorrelation function estimated with 16 000 trajectories. An exponentially divergent behavior due to strong chaos is apparent in the later time.

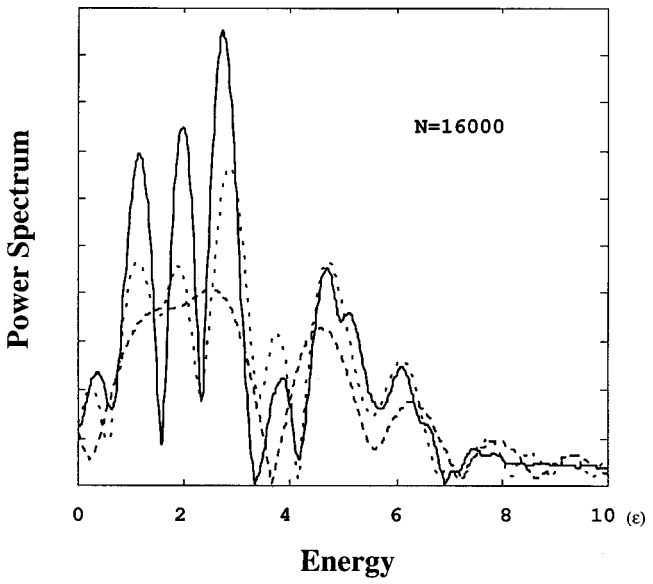

FIG. 6. The power spectra from the autocorrelation function in the IVR in absolute units. The solid curve, short-chained, and long-chained curves represent the Fourier transforms of time intervals $[0,40.96\tau]$, $[40.3\tau,40.96\tau]$, and $[40.6\tau,40.96\tau]$, respectively.

caustics. The exponential growth of the amplitude factor brings two difficulties into the calculation: (1) The resultant Fourier spectra should form Lorentzian peaks at best rather than a delta-functionlike spikes. (2) More seriously, one has to give up continuing the calculation of the correlation function itself due to the numerical overflow.

To illustrate the divergence of the autocorrelation function in the IVR, we show in Fig. 5 a relatively short time evolution of $C(t)=\langle\Psi(0)|\Psi(t)\rangle$ of Eq. (41) $(0<t<6\tau)$. Recall that the time interval 6τ is quite short and is comparable to the periods of the normal modes (see Table 1). Figure 6 displays the Fourier spectra of the time-correlation function taken in three different time intervals; the solid, the short dashed, and the long dashed curves representing the power spectrum of the Fourier transformation of $C(t)$ for $0<t<40.96$, $40.3<t<40.96$, and $40.6<t<40.96$, respectively. The evolution time $t\sim 40.96\tau$ has been a limit of the present IVR calculation that the SADF can offer.

To quantize a relatively weak chaotic system, Kay proposed a method in which strongly chaotic trajectories are all abandoned if the pre-exponential factor exceeds a threshold value predetermined [46]. However, this procedure is unlikely to work in our system, since almost all the trajectories have uniformly a diverging contribution and should be forced to be removed from the calculation (see Fig. 3). Thus, we may conclude that it is impossible to quantize a highly chaotic system like ours by a straightforward application of the IVR. By contrast, the final value representation (FVR) of Eq. (40) must be more appropriate because contributions from unstable trajectories damp due to the inverse form of the pre-exponential factor $|\partial q_t/\partial q_0|^{-1/2}$.

2. Final value representation and divergence due to caustics

Apparent difficulties adherent to the FVR, on the other hand, are (1) there is no guarantee whether the integration points q_t in Eq. (40) give good quadrature points (recall that p_0 is fixed as an initial condition) and (2) it is suffered from divergence at caustic points. As for the first item, however, it is expected that q_t in a strongly chaotic system are randomly distributed in space, so random that they may be regarded as sampling points for Monte Carlo integration. We therefore approximate the FVR correlation function using such a Monte Carlo-type summation over q_t without any quadrature weight.

Figure 7 shows the behavior of the pre-exponential factors $D^{-1/2}\equiv|\partial q_t/\partial q_0|^{-1/2}$ in a logarithmic plot versus time ($\log_{10}D^{-1/2}$ at rather long interval grid points has been connected with straight lines). In Fig. 7(a), a typical example of those of low-energy trajectories for $0<t<10\tau$ (the energies are 0.05ε and 0.20ε) are shown. The signatures of singularities due to caustics are seen quite frequently. These singularities obviously mar the calculation of the correlation function. On the other hand, the typical behavior of the pre-exponential factors of relatively high-energy trajectories (1.12ε and 3.82ε) are shown in Fig. 7(b) for $0<t<45\tau$ along with that for 0.20ε for comparison. It appears on one hand that the exponential decrease of $|\partial q_t/\partial q_0|^{-1/2}$ due to chaos *practically* suppresses the divergence due to caustics. On the other hand, $D^{-1/2}$ under too strong chaos becomes so small very quickly that it cannot make an effective contribution to the correlation function $C(t)$.

A natural tactic to cope with this tough situation should be as follows: (i) First remove the bad effects arising from the singularity at caustics by imposing a cutoff condition on the FVR and then (ii) calculate $C(t)$ to extract a spectrum. This spectrum will be made up by trajectories of appropriately weak chaos. This is because $D^{-1/2}$ of strongly chaotic trajectories damp for themselves and trajectories of too weak chaos, which cannot cancel the singularity at caustics, must

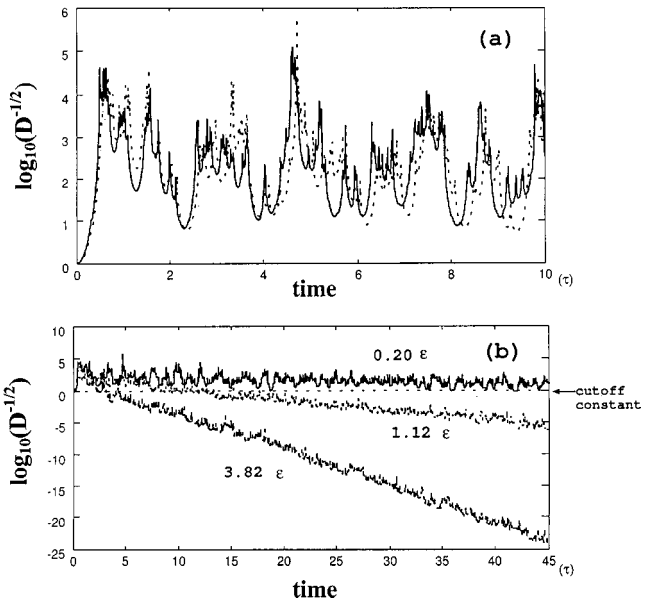

FIG. 7. (a) A typical time evolution of the amplitude factor in the FVR for trajectories of energy as low as 0.05ε (solid curve) and 0.20ε (dotted curve). (b) Exponentially diminishing of the relevant amplitude factor for higher-energy trajectories. (Time in units of τ.)

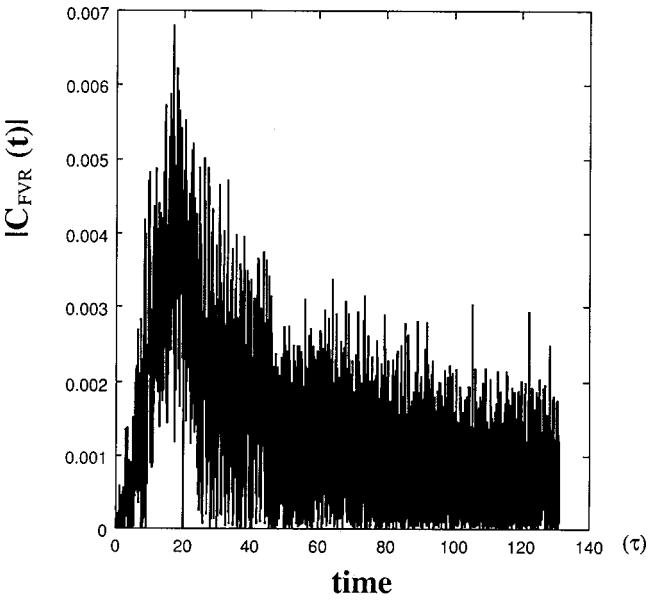

FIG. 8. The absolute value of the correlation function in the FVR with the cutoff. (Time in units of τ.)

be cut off. The spectrum arising from low-energy trajectories, which are either regular (nonchaotic) or very weakly chaotic in the above sense, will be recovered later with use of the IVR. The very high-energy spectrum will not be produced anyway in the present procedure. We set a cutoff condition so that all the contributions from $D^{-1/2}>1.0$ is simply set to zero.

We now report the resultant spectra that have been obtained by means of the FVR with the cutoff. The time-correlation functions of Eq. (47) for the initial wave-packet Eq. (48) have been carried out with 16 000 trajectories running up to a time $T=140\tau$. The trajectories, their associated stability matrix, and so on have been integrated by means of the locally analytic integrator [41]. 140τ is short to cover the typical time scale of the wandering motions ($0.6\varepsilon<E<2.5\varepsilon$), but is about 30 times as long as the periods of normal modes and the swinging mode (see Table I for the normal mode and Fig. 2).

The time-correlation function based on Eq. (47), which is denoted as $C_{FVR}(t)$, is shown in Fig. 8. We also have calculated the correlation function, Eq. (46), in which the atoms are treated as boson ($\varepsilon_i=1$). It turns out numerically that the effect of the permutation is negligibly small in this energy range. The difference between Eqs. (47) and (46) has been only about 1%. This is because dynamics in the relevant energy region is utterly dominated by the swinging motion or because trajectories are confined in a basin. It is observed that $C_{FVR}(t)$ is very small for $t<5\tau\sim10\tau$, which suggests that the cutoff condition (rejection when $D^{-1/2}>1$) may work too hard in the early time. Incidentally, a reasonable convergence of the correlation function with respect to the number of trajectories has been attained with the use of 16 000 trajectories.

Figure 9 shows the resultant energy spectra of $C_{FVR}(t)$ thus obtained. Noticeable difference has not been obtained in the boson spectrum. Two of the distinct peaks are seen around 0.83ε and 1.26ε, which should have arisen from the swinging motion, namely, $0.6\varepsilon<E<2.5\varepsilon$. The broad peak at $\sim1.26\varepsilon$ suggests that it may consist of nearly degenerate

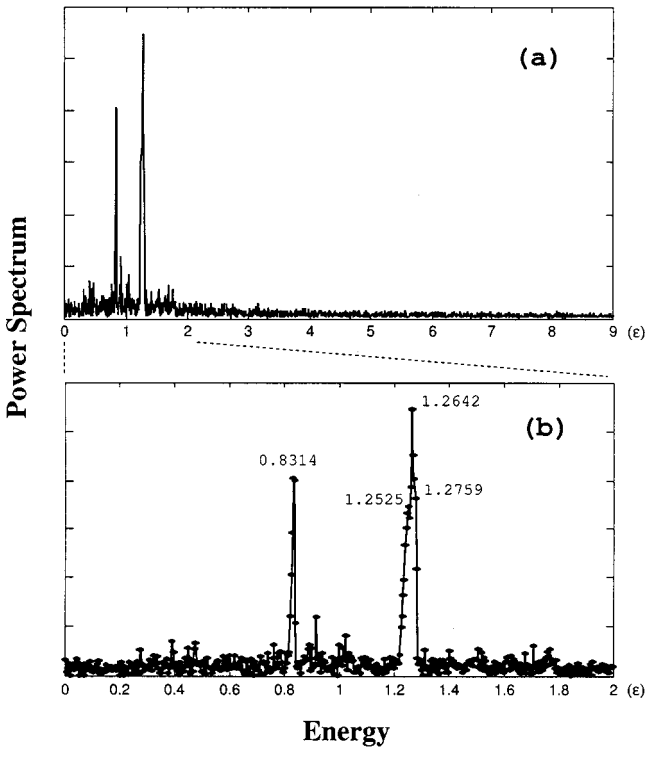

FIG. 9. Energy spectrum in the FVR with the cutoff (setting zero when $D^{-1/2}>1$), which eliminates the low-energy components. (Energy in units of ε.) Also, the high-energy spectrum cannot be produced by the FVR, since the amplitude factors $D^{-1/2}$ are quickly damped to zero due to strong chaos.

peaks. It is important to analyze how these lines are formed. This aspect will be discussed in greater detail in our future publication.

3. Recovery of the low-energy contributions in IVR with a cutoff

As stated above, it is practically impossible for both the IVR and FVR to produce good spectra arising from high-energy trajectories that are of large K entropy. On the other hand, the low-energy trajectories may be well treated by the IVR as long as their instability is small enough. We, hence, try to recover information from the low-energy trajectories including those that have been cut off in the FVR by imposing a condition of rejection if $D^{-1/2}>1$. In doing so, we note that the amplitude factor $D^{1/2}$ associated with even a chaotic trajectory is still oscillatory even though its global feature is divergent. More precisely, $D^{1/2}$ changes in an oscillatory manner between zero and an exponentially diverging value. Hence, one may be able to extract a ''periodic nature'' from a chaotic trajectory by taking account of $D^{1/2}$ only in time intervals during which it takes small values. As a practical procedure, we nullified the contributions when $D^{1/2}>1$ is satisfied. (Note, however, that the maximum value of $D^{1/2}$ eventually overflows in the computer, which disables continuation of the computation. Hence, even with this prescription, the time length for the Fourier transform of the correlation function is limited.) The energy spectrum thus attained in the IVR is shown in Fig. 10. Three panels display the Fourier spectra arising from three different time intervals, namely, (a) $100<t<131$, (b) $50<t<131$, and (c) $0<t<131$. Very complicated spectral feature has come up. The Lindemann index in Fig. 1 indicates that the dense spectrum below the energy about 0.7ε should arise from intrabasin motions in the PBP basin.

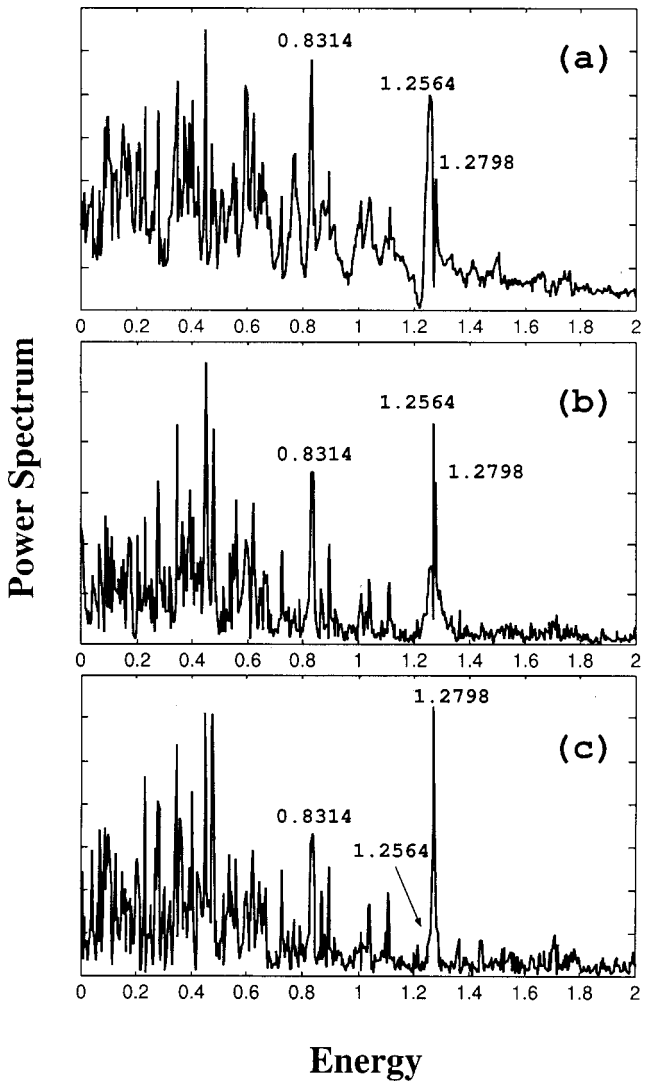

FIG. 10. Energy spectrum in the IVR, recovering the low-energy components of $D^{1/2}<1$. (Energy in units of ε.) The spectra in the panels (a), (b), and (c) have been obtained from time intervals $[100\tau,131\tau]$, $[50\tau,131\tau]$, and $[0\tau,131\tau]$, respectively.

IV. AMPLITUDE-FREE CORRELATION FUNCTION

By making use of both the initial and final representations of the ADF, we have managed to extract some of the vibrational spectral lines in the energy range where the exponential growth of $|\partial q_t/\partial q_0|^{1/2}$ is sufficiently slow. It is still true, however, that the amplitude factor common to the semiclassical theories blocks us to proceed further. We therefore apply a representation of an approximate correlation function that has been devised in the companion paper [31], in which such a troublesome amplitude factor is not present. Very recently, Shao and Makri have developed a semiclassical theory to estimate a general correlation function in their own form that is also free of the amplitude factor (prefactor) [47]. Our theoretical scheme is different from theirs and no comparative study is given here.

A. Correlation function

A minimal review for the correlation function we are going to apply is given first [31]. We begin with a rather peculiar looking but general form of the correlation function represented in terms of the ADF, namely,

$$
\begin{aligned}
C_{p_0}(s,t)=\langle\Psi_{p_0}(s)|\Psi_{p_0}(t)\rangle=\int \exp\Big[&\frac{i}{\hbar}S_2(q_t,p_0,t)\\
&-\frac{i}{\hbar}S_2(q_t,p_0,s)\Big]F^*(q_t,s)F(q_t,t)dq_t\\
=\int\int\ &\delta(q_s-q_t)F^*(q_{01},0)\\
&\times F(q_{02},0)\exp\Big[\frac{i}{\hbar}S_1(q_t,q_{02},t)+\frac{i}{\hbar}p_0q_{02}\\
&-\frac{i}{\hbar}S_1(q_s,q_{01},s)\\
&-\frac{i}{\hbar}p_0q_{01}\Big]dq_{01}^{1/2*}dq_{02}^{1/2}dq_s^{1/2}dq_t^{1/2*}. \qquad (49)
\end{aligned}
$$

In this expression, the square root of the volume element like $dq_t^{1/2}$ is defined as [31]

$$dq_t = dq_t^{1/2} dq_t^{1/2*} \tag{50}$$

under two rules: One is

$$dq_t^{1/2} = \exp\left[i \frac{\pi}{2} N(q_t) \right] |dq_t|^{1/2}, \tag{51}$$

where $N(q_t)$ is the sum of zeros up to the degeneracy of the following determinant picked up by the determinant

$$\frac{\partial q_t}{\partial q_{t=X}} \tag{52}$$

along a classical path. It is convenient to set the reference of time $t=X$ at a far remote past, symbolically denoted as $X = -\infty$. The other one is

$$F(q_t,t) dq_t^{1/2} = F(q_0,0) dq_0^{1/2}, \tag{53}$$

which is to be applied only when the two points are connected by a trajectory.

From the above expression, a useful representation of the correlation function may be extracted by setting $s=-t$, $p_0 = 0$, and $q_{01}=q_{01}$, resulting in

$$\tilde{C}_0(-t,t) = \int\int \delta(q_{-t} - q_t) F^*(q_{01},0) F(q_{01},0) \exp\left[\frac{i}{\hbar} S_1(q_t,q_{01},t) - \frac{i}{\hbar} S_1(q_{-t},q_{01},-t) \right] dq_{01}^{1/2*} dq_{01}^{1/2} dq_{-t}^{1/2} dq_t^{1/2*}, \tag{54}$$

where a trajectory now connects q_{-t} and q_t in such a way that

$$q_{-t}(q_{01},p_0=0) = q_t(q_{01},p_0=0), \tag{55}$$

where $q_t(q_{01},p_0)$ is an end point in configuration space at time t of a trajectory starting from (q_{01},p_0) at $t=0$. After a simple manipulation, $\tilde{C}_0(-t,t)$ appears to be a simpler form

$$\tilde{C}_0(-t,t) = \int dq_{01} |F(q_{01},0)|^2 \exp\left[2\frac{i}{\hbar} S_1(q_t,q_{01},t) - i\frac{\pi}{2} M(q_{-t} \to q_t) \right], \tag{56}$$

where the Maslov index is defined such that $M(q_{-t} \to q_t) = N(q_t) - N(q_{-t})$. In this expression, we notice that the annoying amplitude factor, such as $|\partial q_t / \partial p_0|^{-1/2}$ (exponentially diminishes) or $|\partial q_t / \partial q_{01}|^{1/2}$ (exponentially grows), disappears. Note, however, that the Maslov index does appear in the correlation function. We may call Eq. (56) an intermediate representation, since the trajectories are specified at the middle point $t=0$ in the time interval $[-t,t]$.

The energy spectra extracted from the correlation function of Eq. (56)

$$\begin{aligned} S(E) &= \frac{2}{T} \mathrm{Re} \lim_{T\to\infty} \int_0^{T/2} \tilde{C}_0(-t,t) \exp\left(2\frac{i}{\hbar} Et \right) dt \\ &= \frac{2}{T} \lim_{T\to\infty} \int_0^{T/2} dt \int dq_{01} |F(q_{01},0)|^2 \cos\left[\frac{2}{\hbar} S_1(q_t,q_{01},t) - \frac{\pi}{2} M(q_{-t} \to q_t) + \frac{2}{\hbar} Et \right] \end{aligned} \tag{57}$$

does not have a formal distinction between chaotic and integrable systems. It is well established that the energy spectra in integrable systems are quantized in terms of information only of the action integral and the Maslov index, as typically realized in the EBK condition. On the other hand, it is never trivial that those spectra arising from Eq. (57) cover the entire spectrum, since $\tilde{C}_0(-t,t)$ is an extraction from the full correlation function. The condition considered in $\tilde{C}_0(-t,t)$ that all the trajectories are fixed at $p_0=0$ at $t=0$ must be appropriate to represent standing or stationary waves, since standing waves are generally formed in a fixed boundary.

B. Spectra

An application of the above amplitude-free correlation function is presented below to see how the above spectra are improved. Before that, we have numerically confirmed using a one- and two-dimensional Morse oscillators that $\tilde{C}_0(-t,t)$ actually gives spectral lines at correct energy values. Also, the exact quantum-mechanical spectra for the modified Hénon-Heiles system high in the chaotic energy range have been accurately reproduced [48]. On the other hand, the amplitudes of these spectral lines (or the envelopes) are deformed to some extent from the true one that is expected from the full propagation of the initial wave packet of Eq. (25). This is not surprising in view of the definition of $\tilde{C}_0(-t,t)$.

Since $\tilde{C}_0(-t,t)$ does not involve the diverging or diminishing amplitude factor in it, one may run the trajectories to compute $\tilde{C}_0(-t,t)$ for a far longer time than the standard correlation functions considered in the preceding section. For instance, $t=131\tau$ is the longest we could manage in the IVR as described in the preceding section, while no numerical problem has occurred in $\tilde{C}_0(-t,t)$ even for $t>262\tau$. Consequently, spectral lines with far narrower widths, practically ''line spectra,'' may be obtained, which is in marked contrast to the previous spectra. We thus check the convergence of the spectrum with respect to the time length (T) of the Fourier transform with $N=6000$. Figure 11 shows three spectra arising from $T=66\tau$, 131τ, and 262τ. No qualitatively significant difference between the spectra of $T=131\tau$ and 262τ is noticed. Thus, the spectrum of $T=262\tau$ must be long enough to judge that a convergence has been practically attained.

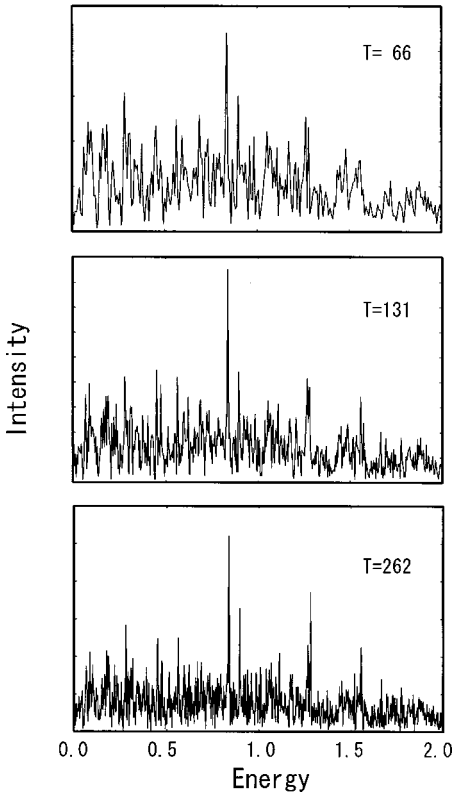

FIG. 11. Convergence of the spectrum based on the amplitude-free correlation function with respect to the time length of the Fourier transform. (Energy in units of ε.) The upper, middle, and lower panels display the spectra arising from $T=66\tau$, 131τ, and 262τ, respectively. The number of trajectories is 6000.

We next check the convergence of $\tilde{C}_0(-t,t)$ with respect to the number of classical trajectories. Since there is no rigorous method to judge whether the full convergence is attained, all we may do here is to look at the behavior of $\tilde{C}_0(-t,t)$ as a function of N examining the invariance of the spectrum with respect to an increase of N. In Fig. 12, we compare the spectra arising from $\tilde{C}_0(-t,t)$ with $N=4000$ and $N=6000$. It turns out that an increase of the trajectories from $N=4000$ to 6000 makes virtually no significant change in the spectral feature. Thus, we regard that the spectrum of $N=6000$ as the converged spectrum.

Finally, we compare, in Fig. 13, the spectrum arising from the FVR in the ADF, the upper panel, and that based on $\tilde{C}_0(-t,t)$, the lower panel. The two prominent peaks in the FVR have been well reproduced by the $\tilde{C}_0(-t,t)$. This fact clearly evidences that there are spectral lines arising from strong classical chaos, for which the magnitude of the amplitude factor, except for the Maslov phase thereof, does not make an essential contribution to quantization. This is impressive if we recall again that the individual spectral lines arising from each periodic orbit necessarily result in a Lorentzian-like shape, the width of which is given by the imaginary part of the stability exponent [49–51].

Furthermore, the $\tilde{C}_0(-t,t)$ spectrum bears many relatively high peaks along with the bushlike features. As stated above, these features are not lowered either by increasing the number of trajectories or by lengthening the run time of the correlation functions. Nonetheless, more study should be necessary to assign these spectral lines. Another important point to note here is that we do not see prominent peaks in the high-energy region, where isomerization should be dominant in classical mechanics. This aspect will be one of the most intensive analyses in our forthcoming study on quan-

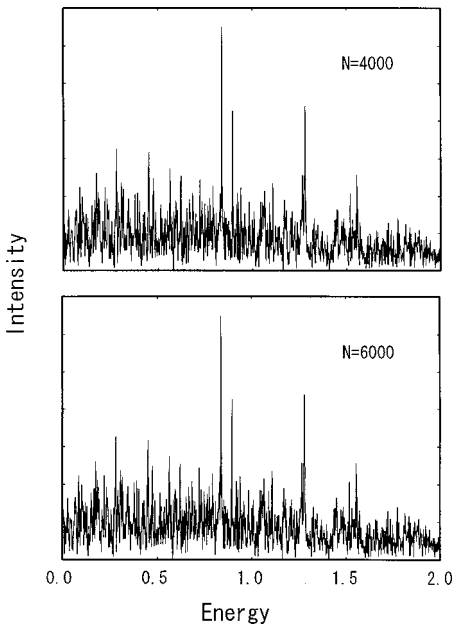

FIG. 12. Convergence of the spectrum based on the amplitude-free correlation function with respect to the number of trajectories. (Energy in units of ε.) The upper panel shows the spectrum with 4000 trajectories, while the lower one with 6000 trajectories.

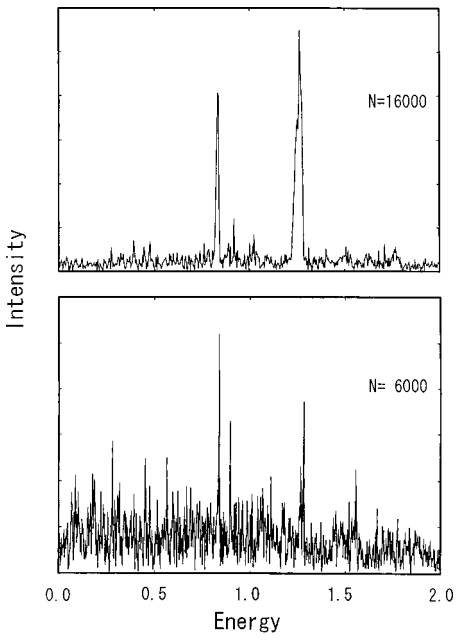

FIG. 13. The final energy spectrum based on the amplitude-free correlation function, the lower panel. (Energy in units of ε.) The upper panel shows the spectrum given by the FVR.

tum and classical correspondence [48].

V. CONCLUDING REMARKS

We have studied semiclassical spectrum of vibrational motion of M_7 cluster, the classical dynamics of which is highly and uniformly chaotic. The presence of strong chaos makes it extremely hard to calculate the spectrum. Various conditions on which to carry out semiclassical evaluation of the chaotic spectrum have been explored. In particular, the roles of singularities due to chaos and caustics in the IVR and FVR have been closely examined. To remove highly chaotic components arising from high-energy trajectories, one needs to impose an appropriate cutoff condition. The relatively low-energy components may be evaluated using the IVR.

A simple and practical method to incorporate the particle permutation into the correlation function has also been presented. The effect of the particle permutation could not be clearly observed in this study, simply because we were only successful to access the spectrum of low-energy isomerization, for which only the swinging motion is dominant. If we could have well-treated high-energy trajectories of the wandering motion, the permutation should have shown its prominent role.

Nevertheless, the spectrum we could obtain by use of both the IVR and FVR is limited in an energy range where the exponential growth of the amplitude factor in the IVR is sufficiently slow. We therefore applied a correlation function that is free of the amplitude factor but with the Maslov index being involved. Much finer spectrum than the above FVR and IVR has been obtained. The most prominent peaks are nonetheless reproduced by all the representations. The spectrum based on the amplitude-free correlation function is what we can do best at the present moment.

The analysis of the spectral peaks has not yet been performed. For instance, the energy $E=1.28$ at which the most significant peak is in the domain of the liquidlike phase, where most of the trajectories should undergo isomerization. Unfortunately, however, the analysis is not necessarily easy, and this aspect will be discussed in full details in our future publication [48].

ACKNOWLEDGMENTS

This work has been supported in part by the Grant-in-Aid from the Ministry of Education, Science, and Culture of Japan. We are grateful to Professor W. H. Miller for continuous discussions on the ADF and the amplitude-free correlation function.

[1] For extensive reviews, see R. S. Berry, Chem. Rev. **93**, 2379 (1993); R. S. Berry, Int. J. Quantum Chem. **58**, 657 (1996); K. D. Ball, R. S. Berry, R. E. Kunz, F.-Y. Li, A. Proykova, and D. J. Wales, Science **271**, 963 (1996). See, also, D. J. Wales, *ibid.* **271**, 925 (1996).
[2] C. Seko and K. Takatsuka, J. Chem. Phys. **104**, 8613 (1996).
[3] K. Takatsuka and C. Seko, J. Chem. Phys. **105**, 10 356 (1996).
[4] C. Seko and K. Takatsuka, J. Chem. Phys. **108**, 4924 (1998).
[5] C. Seko and K. Takatsuka, J. Chem. Phys. **109**, 4768 (1998).
[6] K. Takatsuka and C. Seko, J. Chem. Phys. **110**, 3263 (1999).
[7] T. Yanao and K. Takatsuka, Chem. Phys. Lett. **313**, 633 (1999).
[8] K. Takatsuka and T. Yanao, J. Chem. Phys. **113**, 2552 (2000).
[9] D. M. Leitner, R. S. Berry, and R. M. Whitnell, J. Chem. Phys. **91**, 3470 (1989).
[10] C. Chakravarty, R. J. Hinde, D. M. Leitner, and D. J. Wales, Phys. Rev. E **56**, 363 (1997).
[11] S. W. Rick, D. L. Leitner, J. Doll, D. L. Freeman, and D. D. Frantz, J. Chem. Phys. **95**, 6658 (1991).
[12] J. P. Neirotti, F. Calvo, D. L. Freeman, and J. D. Doll, J. Chem. Phys. **112**, 10 340 (2000), and references therein.
[13] R. O. Weht, J. Kohanoff, and C. Chakravarty, J. Chem. Phys. **108**, 8848 (1998).
[14] M. V. Berry and K. E. Mount, Rep. Prog. Phys. **35**, 315 (1972).
[15] W. H. Miller, Adv. Chem. Phys. **25**, 69 (1974); **30**, 77 (1975).
[16] L. S. Schulman, *Technique and Applications of Path Integration* (Wiley, New York, 1981).
[17] V. P. Maslov and M. V. Feodoriuk, *Semi-Classical Approximation in Quantum Mechanics* (Reidel, Dordrecht, 1981).
[18] M. S. Child, *Semiclassical Mechanics with Molecular Approximations* (Clarendon, Oxford, 1991).
[19] P. Gaspard, D. Alonso, and I. Burghardt, Adv. Chem. Phys. **90**, 105 (1995).
[20] M. L. Brewer, J. S. Hulme, and D. E. Manolopoulos, J. Chem. Phys. **106**, 4832 (1997).
[21] K. Takatsuka and A. Inoue, Phys. Rev. Lett. **78**, 1404 (1997); A. Inoue-Ushiyama and K. Takatsuka, Phys. Rev. A **59**, 3256 (1999); **60**, 112 (1999).
[22] R. J. Hinde, R. S. Berry, and D. J. Wales, J. Chem. Phys. **96**, 1376 (1992).
[23] R. J. Hinde and R. S. Berry, J. Chem. Phys. **99**, 2942 (1993).
[24] W. H. Miller, J. Chem. Phys. **53**, 3578 (1970).
[25] X. Sun and W. H. Miller, J. Chem. Phys. **110**, 6635 (1999).
[26] E. J. Heller, J. Chem. Phys. **62**, 1544 (1975); **65**, 4979 (1976).
[27] E. J. Heller, J. Chem. Phys. **94**, 2723 (1991), and references therein.
[28] M. A. Sepulveda and E. J. Heller, J. Chem. Phys. **101**, 8004 (1994); M. A. Sepúlveda and F. Grossmann, Adv. Chem. Phys. **96**, 191 (1996) and references therein.
[29] G. Campolieti and P. Brumer, Phys. Rev. A **50**, 997 (1994); D. Provost and P. Brumer, Phys. Rev. Lett. **74**, 250 (1995).
[30] K. G. Kay, J. Chem. Phys. **100**, 4377 (1994); **100**, 4432 (1994); **101**, 2250 (1994).
[31] K. Takatsuka, the companion paper, Phys. Rev. E **64**, 016224 (2001)
[32] P. A. Braier and R. S. Berry, J. Chem. Phys. **93**, 8745 (1990).
[33] M. R. Hoare and P. Pal, J. Cryst. Growth **17**, 77 (1972); J. Farges, M. F. Faraudy, B. Raoult, and G. Torchet, J. Chem. Phys. **78**, 5067 (1983).

[34] F. H. Stillinger and T. A. Weber, Phys. Rev. A **25**, 978 (1982).
[35] F. G. Amer and R. S. Berry, J. Chem. Phys. **85**, 5943 (1986).
[36] G. Natason, F. G. Amar, and R. S. Berry, J. Chem. Phys. **78**, 399 (1983); R. S. Berry, J. Jellinek, and G. Natanson, Phys. Rev. A **30**, 919 (1984); Chem. Phys. Lett. **107**, 227 (1984); J. Jellinek, T. L. Beck, and R. S. Berry, J. Chem. Phys. **84**, 2783 (1985).
[37] S. Sawada and S. Sugano, Z. Phys. D: At., Mol. Clusters **12**, 189 (1989).
[38] A. J. Lichtenberg and M. A. Lieberman, *Regular and Chaotic Dynamics* (Springer, Berlin, 1992).
[39] K. Takatsuka, Phys. Rev. A **45**, 4326 (1992).
[40] K. Takatsuka, Phys. Rev. Lett. **61**, 503 (1988); K. Takatsuka, Phys. Rev. A **39**, 5961 (1989).
[41] H. Ushiyama, Y. Arasaki, and K. Takatsuka, Chem. Phys. Lett. **346**, 169 (2001).
[42] H. Goldstein, *Classical Mechanics* (Addison-Wesley, New York, 1980).
[43] K. Takatsuka and H. Ushiyama, Phys. Rev. A **51**, 4353 (1995); H. Ushiyama and K. Takatsuka, J. Chem. Phys. **106**, 7023 (1997); **109**, 9664 (1998).
[44] K. Takatsuka, H. Ushiyama, and A. Inoue-Ushiyama, Phys. Rep. **322**, 347 (1999).
[45] M. J. Davis and E. J. Heller, J. Chem. Phys. **75**, 246 (1981).
[46] K. G. Kay, J. Chem. Phys. **101**, 2250 (1994).
[47] J. Shao and N. Makri, J. Phys. Chem. A **103**, 7753 (1999); **103**, 9479 (1999).
[48] K. Hotta and K. Takatsuka (unpublished).
[49] M. C. Gutzwiller, J. Math. Phys. **11**, 1791 (1970); **12**, 343 (1971); *Chaos in Classical and Quantum Mechanics* (Springer, New York, 1990).
[50] R. B. Balian and C. Bloch, Ann. Phys. (N.Y.) **60**, 401 (1970); **85**, 1514 (1974).
[51] K. Takatsuka, Phys. Rev. A **45**, 4326 (1992); Prog. Theor. Phys. **91**, 421 (1994).